Density Functional Approach to Adsorption and Retention of Spherical Molecules on Surfaces Modified with End-Grafted Polymers

M. Borówko, W. Rżysko, S. Sokołowski, and T. Staszewski*

Department for the Modeling of Physico-Chemical Processes, Maria Curie-Skłodowska University, 20-031 Lublin, Poland

Received: December 17, 2008; Revised Manuscript Received: February 2, 2009

A density functional approach to describe adsorption of Lennard-Jones fluids on a surface modified with grafted chains is proposed. The theory is extended to the solute retention in chromatography with chemically bonded phases. The chain molecules are modeled as freely jointed tangent spheres with end segments linked to the surface. The segments interact via Lennard-Jones potential. The effects of grafting density and molecular interactions are discussed. The results are compared with the Monte Carlo simulation data. The theory predicts the most important features of the retention process.

I. Introduction

Polymer layers consisting of chains with one end attached to a surface have been intensively studied in recent years due to their importance as a component of colloid stabilization agents, protective films, adhesives, and so forth.[1−4] The adsorbents covered by chemically bonded polymers are also used as stationary phases in gas chromatography and reversed-phase liquid chromatography.

The properties of the end-grafted chains depend strongly on their structure, which can be categorized as being either a "mushroom" or a "brush", depending on the grafting density. In the "mushroom" structure the chains are isolated and can assume nearly unperturbed dimensions. For higher grafting densities, individual chains begin to overlap and the interchain repulsion causes the polymers to stretch in the direction perpendicular to the surface. The thickness of such a "brush" structure exceeds the unperturbed coil radius. Behavior of grafted chains depends on the solvent quality. For "good solvents", segment−solvent contacts are more favorable than segment−segment contacts, and chains spread. In the "poor solvent" regime, the effective interactions between segments are attractive, resulting in the chain collapse. The understanding of this structural transitions is of considerable practical importance.

One of the first theoretical treatments of chains tethered to a surface was developed by Alexander[5] and de Gennes.[6] The description of polymer brushes was greatly improved by Milner, Witten, and Cates[7−9] who presented an analytical solution of the classical self-consistent field equations for stretched polymer brushes in a good solvent. The self-consistent field theory was then employed by numerous authors to study the tethered polymers in different solvent conditions.[10−17] A further progress in theoretical studies of polymer brushes was made through the so-called single-chain mean-field method.[18−21] According to this method, the statistical mechanics of a single chain is treated exactly, whereas the interaction with the other chains are taken into a mean-field level. In the past decade, several versions of the density functional approach were applied to describe the end-grafted chains. McCoy and co-workers[21−25] and Wu et al.[26,27] considered behavior of the chains in an implicit solvent, as well as in "continuum solvent approximation". Recently, the approach of Wu et al.[26,28−30] was applied to describe adsorption of hard-sphere mixtures[31] and one-component Lennard-Jones fluid[32,33] onto surfaces modified by preadsorbed chain molecules. We should also mention that in numerous works[34−46] computer simulations were used to study the systems involving tethered chains. The significant aim of simulations was to explain mechanism of structural transitions in grafted polymer films.

As mentioned, adsorbents with attached polymers are widely used as column packings in chromatography. The reversed-phase liquid chromatography constitutes one of the most important techniques for separating chemicals. It is estimated that about 90% of all analytical separations on low molecular weight samples are carried out using this technique.[47] Further improving the method requires detailed understanding of separation process at molecular level. Therefore, in recent years a great deal of research has focused on this problem.[48] A few theoretical treatments of the solute retention have been proposed.[48−51] These approaches were based on relatively simple lattice models of bonded phases. More realistic models appeared to be far too complex to allow for an analytical treatment. For this reason, the most recent studies have been conducted using computer simulation techniques.[52−63] Molecular dynamics (MD) simulations were carried out for the systems where no solvent was explicitly involved.[52−55] A number of MD simulations were also performed for different bonded phases and water/methanol or water/acetonitrile as solvents.[56−58] Quite recently, the results of isobaric−isothermal Gibbs ensemble Monte Carlo simulations based a complex and quite realistic model of the chromatographic system were reported.[59−63] The aim of these studies was to investigate how various parameters affect the structural properties of stationary phases and the solute retention.

In this work, we apply the density functional approach proposed in our previous papers[31,33] to describe adsorption of one-component Lennard-Jones fluid on polymer brushes. The relevant Monte Carlo simulations have been carried out to test the theory and to investigate the structure of the interface. We propose here the density functional treatment of the solute retention in chromatographic separation involving chemically bonded phases. The paper is organized as follows. In section II we describe our model. Then in section III we present the density functional theory. The simulation methodology is briefly

* Corresponding author. E-mail: tomo@heksan.umcs.lublin.pl.

10.1021/jp811143n CCC: $40.75
Published on Web 03/18/2009

reviewed in section IV. The results are presented and discussed in section V and section VI gives the summary.

II. Theory

Model. We study adsorption of spherical molecules (F) onto a flat surface covered by preadsorbed chain molecules (P). The linear chains are composed of M tangentially jointed segments of the came diameter $\sigma^{(P)}$. The chain connectivity is enforced by the bonding potential V_B in the form[28]

$$\exp[-\beta V_B(\mathbf{R})] = \prod_{i=1}^{M-1} \delta(|\mathbf{r}_{i+1} - \mathbf{r}_i| - \sigma^{(P)})/4\pi(\sigma^{(P)})^2 \quad (1)$$

where $\beta = 1/kT$, $\delta(r - \sigma^{(P)})$ is the Dirac function and $\mathbf{R} \equiv (\mathbf{r}_1, \mathbf{r}_2, ..., \mathbf{r}_M)$ denotes a set of coordinates describing the segment positions.

Each polymer molecule contains one surface-binding segment located at its end that interacts with the surface via the potential

$$\exp[-\beta v_{s1}(z)] = C\delta(z - \sigma^{(P)}/2) \quad (2)$$

In the above, z is a distance from the surface, $\delta(z - \sigma^{(P)}/2)$ is the Dirac function and C is a constant. The potential (2) implies that the first segment can move in the $z = \sigma^{(P)}/2$ plane. This means that the considered model does not exactly correspond to a model of chemisorbed chains, where grafted ends of polymer molecules are "anchored", and their grafted ends are strictly fixed at active sites on the wall. The remaining segments of the polymer are "neutral" with respect to the surface; i.e., the hard-wall potentials are assumed for interactions between these segments and the wall. The hard-wall potential is also used to describe the interaction of a spherical molecule with the substrate, thus

$$v^{(i)}(z) = \begin{cases} \infty & z \le \sigma^{(i)}/2 \\ 0 & \text{otherwise} \end{cases} \quad (3)$$

where i = F, P and $\sigma^{(F)}$ is the diameter of spherical molecules. Interactions between all segments of chains and fluid molecules are given by the Lennard-Jones potential

$$u^{(ij)}(r) = 4\varepsilon^{(ij)}[(\sigma^{(ij)}/r)^{12} - (\sigma^{(ij)}/r)^6] \quad (4)$$

where $\sigma^{(ij)} = 0.5(\sigma^{(i)} + \sigma^{(j)})$, i,j = P,F and $r = |\mathbf{r}_{12}| = |\mathbf{r}_1 - \mathbf{r}_2|$.

In the model under study the grafting density, ρ_p, per surface area A, is fixed. Thus, the local density of the first segment at the wall also remains fixed. On the other hand, at distances from the surface greater than $(M + 1/2)\sigma^{(P)}$ polymer molecules are not present. The adsorption system composed of grafted chains and spherical molecules is in equilibrium with a reservoir containing only spherical molecules. In such a situation, one should use a kind of semigrand canonical ensemble to describe the system.

III. Density Functional Theory

The density functional theory employed here is based on the theory developed by Yu and Wu.[28] The interactions between segments and spherical molecules are treated in a perturbational manner. The potential $u^{(ij)}$ (eq 4) is divided into the repulsive (reference) and attractive (perturbation) parts. Then, the repulsive term is approximated by the hard-sphere potential with the effective hard-sphere diameter $d^{ij} = \sigma^{(ij)}$. The Weeks−Chandler−Anderson scheme[64] is used to divide the potential $u^{(ij)}$ and its attractive part is given by

$$u_{att}^{(ij)}(r) = \begin{cases} -\varepsilon^{(ij)} & r < 2^{1/6}\sigma^{(ij)} \\ u^{(ij)}(r) & r \ge 2^{1/6}\sigma^{(ij)} \end{cases} \quad (5)$$

Following previous papers[28−30] the free energy functional is decomposed as the sum of ideal and excess terms, $F = F_{id} + F_{ex}$. The excess free energy is the sum $F_{ex} = F_{hs} + F_c + F_{att}$, where F_{hs} is the term due to the hard-sphere contribution, F_c is the Helmholtz free energy due to chain connectivity, and the term F_{att} describes attractive interactions in the system. The ideal part of the free energy functional is given by

$$\beta F_{id} = \beta \int d\mathbf{R}\, \rho^{(P)}(\mathbf{R}) V_B(\mathbf{R}) + \int d\mathbf{R}\, \rho^{(P)}(\mathbf{R}) [(\ln(\rho^{(P)}(\mathbf{R})) - 1] + \int d\mathbf{r}\, \rho^{(F)}(\mathbf{r}) [(\ln(\rho^{(F)}(\mathbf{r})) - 1] \quad (6)$$

where $\rho^{(P)}(\mathbf{R})$ and $\rho^{(F)}(\mathbf{r})$ are the local densities of chains and spherical molecules, respectively. In order to proceed to the evaluation of the excess free energy contributions, we introduce the local densities of particular segments, $\rho_{s,j}^{(P)}(\mathbf{r})$, and the total segment density, $\rho_s^{(P)}(\mathbf{r})$, via[26−33]

$$\rho_s^{(P)}(\mathbf{r}) = \sum_{j=1}^{M} \rho_{s,j}^{(P)}(\mathbf{r}) = \sum_{j=1}^{M} \int d\mathbf{R}\, \delta(\mathbf{r} - \mathbf{r}_j)\rho^{(P)}(\mathbf{R}) \quad (7)$$

Because the theory we deal with was discussed in numerous works,[26−33] only its basic points are outlined here. The excess free energy terms due to hard-sphere contribution, F_{hs}, and due to the chain connectivity, F_c, are evaluated from the fundamental measure theory and from the first-order theory of Wertheim by using eqs 9 and 16−19 from ref 28. For the sake of brevity, we do not repeat them here.

The free energy resulting from the attractive interactions is obtained within the mean field approximation, so we have

$$F_{att} = \frac{1}{2}\int d\mathbf{r}_1\, d\mathbf{r}_2\, \rho^{(F)}(\mathbf{r}_1)\rho^{(F)}(\mathbf{r}_2)u^{(FF)}(\mathbf{r}_{12}) + \int d\mathbf{r}_1\, d\mathbf{r}_2\, \rho^{(F)}(\mathbf{r}_1)\rho_s^{(P)}(\mathbf{r}_2)u^{(FP)}(\mathbf{r}_{12}) + \frac{1}{2}\int d\mathbf{r}_1\, d\mathbf{r}_2\, \rho_s^{(P)}(\mathbf{r}_1)\rho_s^{(P)}(\mathbf{r}_2)u^{(PP)}(\mathbf{r}_{12}) \quad (8)$$

The equilibrium density profiles of chains and spherical molecules can be evaluated by minimization the thermodynamic potential in the ensemble in which the total number of chains is fixed. We have

$$\mathscr{Y} = F[\rho^{(P)}(\mathbf{R}), \rho^{(F)}(\mathbf{r})] + \int d\mathbf{R}\, \rho^{(F)}(\mathbf{r})(v^{(F)}(\mathbf{r}) - \mu^{(F)}) \quad (9)$$

In the above, $\mu^{(F)}$ is the chemical potential of F species. The constancy of the amount of chain particles is given by

$$\int_0^{(M+1/2)\sigma_P} dz\, \rho_{s,j}^{(P)}(z) = \rho_P \tag{10}$$

After calculations described in the previous papers,[31,33] one can evaluate the density profiles from

$$\rho^{(F)}(z) = \exp\{\beta\mu^{(F)} - \beta\lambda^{(F)}(z)\} \tag{11}$$

and

$$\rho^{(P)}(\mathbf{R}) = \tilde{C}\exp\left\{\beta V_B(\mathbf{R}) - \beta \sum_{j=1,M} \lambda_j^{(P)}(z_j)\right\} \tag{12}$$

where

$$\lambda_j^{(P)}(z_j) = \frac{\delta F_{ex}}{\delta \rho_s^{(P)}(z_j)} + v_{sj}^{(P)}(z_j) \tag{13}$$

and

$$\lambda^{(F)}(z) = \frac{\delta F_{ex}}{\delta \rho^{(F)}(z)} + v^{(F)}(z) \tag{14}$$

The segment densities of chain molecules are given by

$$\rho_{s,i}^{(P)}(z) = \tilde{C}\exp[-\beta\lambda_i^{(P)}(z)]G_i^{(L)}(z)G_{M+1-i}^{(R)}(z) \tag{15}$$

where the functions $G^{(P)}(z)$, P = L, R are determined from the following recurrence relations

$$G_i^{(L)}(z) = \int dz' \exp[-\beta\lambda_{i-1}^{(P)}(z)]\frac{\theta(\sigma^{(P)} - |z - z'|)}{2\sigma^{(P)}}G_{i-1}^{(L)}(z') \tag{16}$$

and

$$G_i^{(R)}(z) = \int dz' \exp[-\beta\lambda_{M-i+2}^{(P)}(z)] \times \frac{\theta(\sigma^{(P)} - |z - z'|)}{2\sigma^{(P)}}G_{i-1}^{(L)}(z') \tag{17}$$

for $i = 2, 3,..., M$ and with $G^{(L)}(z) = G^{(R)}(z) \equiv 1$. The constant $\tilde{C}$ is evaluated from eq 10.

The excess adsorption of spherical molecules is given by

$$\Gamma_F = \int (\rho^{(F)}(z) - \rho_b^{(F)})\, dz \tag{18}$$

where $\rho_b^{(F)}$ is a bulk density of the fluid.

In this work, we assumed that all segments and spherical molecules are of the same size $\sigma^{(P)} = \sigma^{(F)} = \sigma$.

IV. Monte Carlo Simulations

The Monte Carlo simulation (MC) method used in the study has been already outlined in our previous paper.[31] Therefore, we shall describe here only the most important points of the simulation algorithm. The simulations were carried out in grand canonical ensemble. A cuboidal box was used with walls located at $z = 0$ and $z = H\sigma$. One surface is a bare hard wall, and the other is a hard wall with attached polymer chains. Two remaining box dimensions, L_x and L_y were kept at 14σ. Standard periodic boundary conditions were applied in x and y directions. The distance between surfaces ($H\sigma$) was large enough, and the bare wall did not restrict the configurations of the grafted chains. A fixed number N_P chain molecules were "anchored" onto the wall. Their end segments were located at $z_0 = \sigma/2$, and the grafting points were randomly chosen on the surface.

The simulations were organized in cycles as follows. Each cycle consisted of two steps: (i) an attempt to change a state of "the living surface" by changing a conformation of randomly selected anchored chain, and (ii) the standard trial move in a grand-canonical simulation for fluid molecules.[65]

The trial conformations of chains were generated using the Rosentbuth configuration-bias method.[66] The attempts of inserting or removing spherical molecules were carried out using the standard Metropolis algorithm.

Each system was equilibrated for 10^6 Monte Carlo cycles, and the production runs last for up to 10^7 Monte Carlo steps. During the production stage we have calculated densities of particular segments and density of spherical molecules. The simulations were performed for chains built of $M = 8$ segments and for $\varepsilon^{(FF)} = \varepsilon$. In other words, the parameters σ and ε were taken as the units of the length and energy, respectively. We define a reduced temperature as $T^* = kT/\varepsilon$. All calculations were performed for $T^* = 1.5$.

Four sets of remaining interaction parameters were considered: (1) $\varepsilon^{(PP)} = \varepsilon^{(FP)} = \varepsilon$; (2) $\varepsilon^{(PP)} = 0.5\varepsilon$, $\varepsilon^{(FP)} = \varepsilon$; (3) $\varepsilon^{(PP)} = \varepsilon$, $\varepsilon^{(FP)} = 1.5\varepsilon$; (4) $\varepsilon^{(PP)} = 0.5\varepsilon$, $\varepsilon^{(FP)} = 1.5\varepsilon$. Three grafting densities were investigated: the low grafting density ($\rho_P\sigma^2 = 0.0998\,72$), the mediate grafting density ($\rho_P\sigma^2 = 0.199\,74$), and the relatively high grafting density ($\rho_P\sigma^2 = 0.299\,62$). The following chemical potentials of the bulk fluid were assumed: $\mu_b^{(F)}/\varepsilon = -3$, -4, and -5.

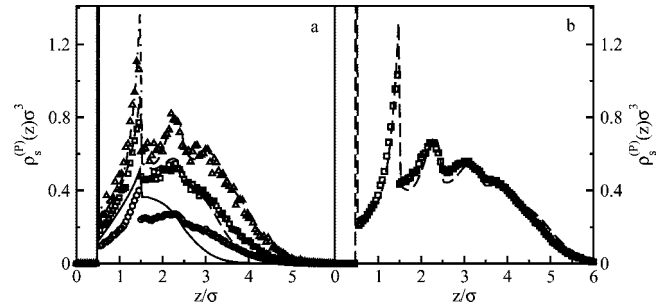

Figure 1. (a) A comparison of theoretical total segment density profiles of polymers (lines) with Monte Carlo simulation data (symbols) for different grafted densities $\rho_P\sigma^2 = 0.099\,872$ (solid line and circles), 0.199 74 (dashed line and squares), and 0.299 62 (dash-dotted line and triangles). Parameters: $\varepsilon^{(FF)} = \varepsilon^{(PP)} = \varepsilon^{(FP)} = \varepsilon$ and $\mu_b^{(F)}/\varepsilon = -5.0$. (b) A comparison of theoretical total segment density profiles of polymers (dashed line) with Monte Carlo simulation data (symbols). Parameters: $\varepsilon^{(PP)} = 0.5\varepsilon$ and $\varepsilon^{(FF)} = \varepsilon^{(FP)} = \varepsilon$, $\mu_b^{(F)}/\varepsilon = -5.0$ and $\rho_P\sigma^2 = 0.299\,62$.

V. Results and Discussion

Density Profiles of End-Grafted Chains. Figures 1 and 2 show density profiles for systems containing end-grafted chains obtained for different parameters characterizing the model. Symbols denote Monte Carlo results, and lines are the profiles calculated using density functional approach. In Figure 1 the density profiles of polymers are presented for gradually increas-

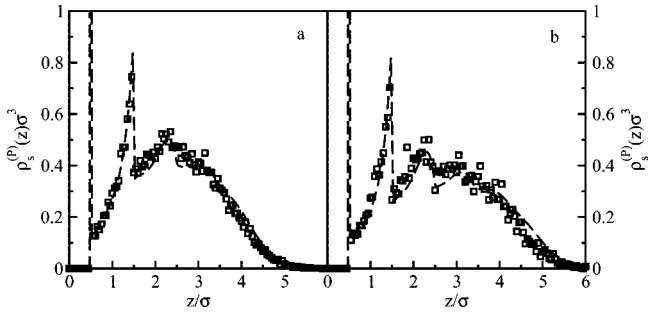

Figure 2. A comparison of theoretical total segment density profiles of polymers (lines) with Monte Carlo simulation data (symbols). (a) Parameters: $\varepsilon^{(FF)} = \varepsilon^{(PP)} = \varepsilon$ and $\varepsilon^{(FP)} = 1.5\varepsilon$, $\mu_b^{(F)}/\varepsilon = -5.0$ and $\rho_P\sigma^2 = 0.199\,74$. (b) Parameters: $\varepsilon^{(PP)} = 0.5\varepsilon$, $\varepsilon^{(FF)} = \varepsilon$, and $\varepsilon^{(FP)} = 1.5\varepsilon$, $\mu_b^{(F)}/\varepsilon = -5.0$ and $\rho_P\sigma^2 = 0.199\,74$.

ing grafting densities. As has been already mentioned the chain density vanishes at distances greater than the maximum brush height D. The "effective" brush height $D_{eff}^* = D_{eff}/\sigma$ depends on the grafting density. An increase of the grafting density causes a rise of the effective brush height. The chains are repelled from the surface and thus they are more stretched. In the case depicted in Figure 1a the values of D_{eff}^* estimated for increasing grafting densities are 4.27, 4.97, and 5.67 for the profiles obtained from theory, and 5.44, 5.58, and 5.87 for the profiles from MC simulations. In part b, the values of D_{eff}^* estimated from theory and simulation are 6.59 and 6.60, respectively.

All profiles exhibit Dirac delta peak at $z = \sigma/2$ that corresponds to the pinned segments. However, the height of these peaks is cut in the relevant figures. The structures of further part of the brushes are different for different parameters. For higher grafting densities the liquidlike structures with peaks corresponding to successive layers of polymer segments are observed. When the grafting density is low the polymer density decreases almost monotonically with the distance from the wall.

Figure 1b presents the chain profile for the highest grafting density and for weaker than in Figure 1a segment−segment interactions. One can see that in this case chains are slightly more extended. Figures 2 also illustrates the influence of the strength of attractive segment−segment interactions on the structure of the grafted polymers. In part a the chain profile for $\varepsilon^{(PP)} = \varepsilon$ is plotted, whereas part b shows the chain profile for weaker interactions between segments, namely for $\varepsilon^{(PP)} = 0.5\varepsilon$. The effective brush height for stronger segment−segment interactions (part a) is $D_{eff}^* = 5.66$ (theory) and 5.71 (simulation) and it is lower than that estimated for the system with weaker segment−segment energy (part b). In the latter case $D_{eff}^* = 6.27$ (theory) and 6.28 (simulation). Comparing suitable profiles from Figures 1 and 2, one concludes that a change in the segment−fluid interaction only slightly affects the brush structure. The density functional theory approximates the Monte Carlo simulation results with a good accuracy for high grafting densities. In the case of low grafting density, the theory predicts a considerably lower polymer density in the outer region of the surface layer than the simulations (see Figure 1).

Adsorption of Lennard-Jones Fluid on Brushes. We begin with the discussion of the density profiles of spherical molecules obtained for different parameters characterizing interactions in the mixture ($\varepsilon^{(PP)}$ and $\varepsilon^{(FP)}$) and for different grafting densities.

Figure 3 presents the results for the first set of the interaction parameters ($\varepsilon^{(PP)} = 1$, $\varepsilon^{(FP)} = 1$). Part a shows a comparison of density profiles for different grafting densities. The relevant profiles of polymers have already been depicted in Figure 1.

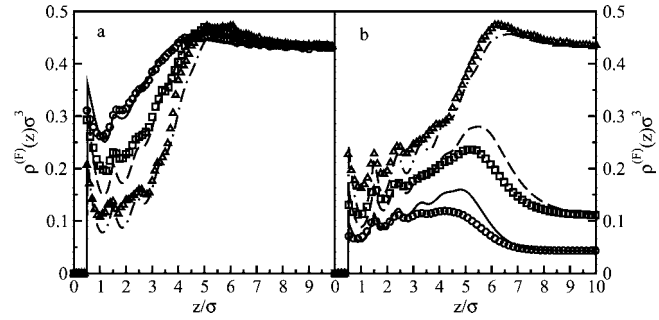

Figure 3. (a) A comparison of theoretical density profiles of adsorbed fluid (lines) with Monte Carlo simulation data (symbols) for different grafted densities $\rho_P\sigma^2 = 0.099\,872$ (solid line and circles), 0.199 74 (dashed line and squares), and 0.299 62 (dash-dotted line and triangles). Parameters: $\varepsilon^{(PP)} = \varepsilon^{(FF)} = \varepsilon^{(FP)} = \varepsilon$ and $\mu_b^{(F)}/\varepsilon\sigma^3 = -3.0$. (b) A comparison of theoretical density profiles of adsorbed fluid (lines) with Monte Carlo simulation data (symbols) for different chemical potentials of fluid $\mu_b^{(F)}/\varepsilon = -5.0$ (solid line and circles), −4.0 (dashed line and squares), and −3.0 (dash-dotted line and triangles). Parameters: $\varepsilon^{(FF)} = \varepsilon^{(FP)} = \varepsilon$, $\varepsilon^{(PP)} = 0.5\varepsilon$, and $\rho_P\sigma^2 = 0.299\,62$.

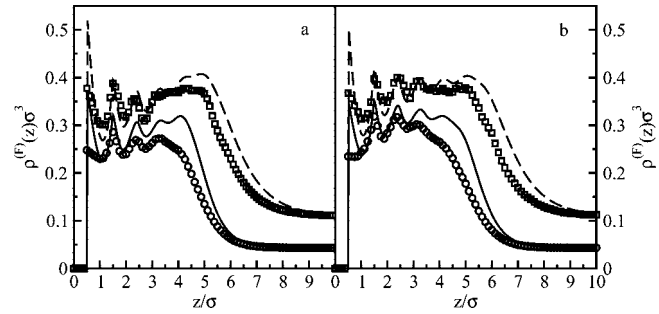

Figure 4. A comparison of theoretical density profiles of adsorbed fluid (lines) with Monte Carlo simulation data (symbols) for different chemical potentials of fluid $\mu_b^{(F)}/\varepsilon = -5.0$ (solid line and circles) and −4.0 (dashed line and squares). (a) Parameters: $\varepsilon^{(PP)} = \varepsilon^{(FF)} = \varepsilon$, $\varepsilon^{(FP)} = 1.5\varepsilon$, and $\rho_P\sigma^2 = 0.199\,74$. (b) Parameters: $\varepsilon^{(PP)} = 0.5\varepsilon$, $\varepsilon^{(FF)} = \varepsilon$, and $\varepsilon^{(FP)} = 1.5\varepsilon$ and $\rho_P\sigma^2 = 0.199\,74$.

One can see that the fluid molecules are adsorbed in the outer region of the brush. The fluid density "at the brush end" slightly increases with an increase of the grafting density. However, inside the core of the bonded phase a deep depletion in the fluid density is observed. This "dewetting effect" is more prevalent for dense polymer films. In Figure 3b the density profiles of the fluid are plotted for the highest grafting density and for different bulk densities. The agreement between Monte Carlo results and theoretical predictions is considerably better for dense fluids.

In Figure 4 the density profiles of spherical molecules calculated for mediate grafting density ($\rho_P\sigma^2 = 0.199\,974$) are presented. In this case strong attractive polymer−fluid interactions have been assumed, $\varepsilon^{(FP)} = 1.5\varepsilon$, so a large number of fluid molecules are located within the brush. The fluid density in the bonded phase is significantly higher than the density in the bulk phase. A change of the segment−segment interactions slightly affects adsorption of spherical molecules, cf. Figure 4a which was evaluated for $\varepsilon^{(PP)} = \varepsilon$ and Figure 4b, obtained for $\varepsilon^{(PP)} = 0.5\varepsilon$. The change of the parameter $\varepsilon^{(PP)}$ is, however, reflected by a certain change in the effective brush height. For the weaker segment−segment attractive interactions the bonded phase extends further out.

Figure 5 depicts the results of Monte Carlo simulations performed for the very low grafting density $\rho_P\sigma^2 = 0.099872$. In part a, the density profiles of the bonded phase and the density profiles of fluid molecules for different segment−segment

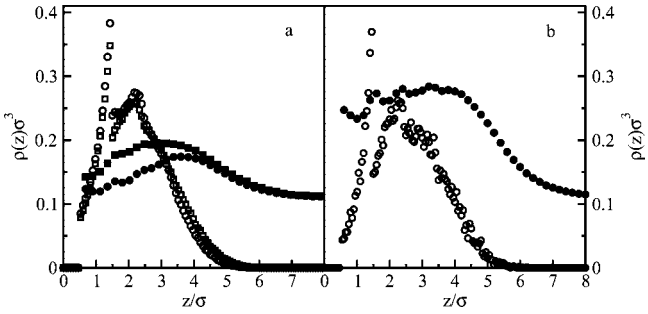

Figure 5. (a) Density profiles of polymers (void symbols, $\rho \equiv \rho_s^{(P)}$) and fluid (solid symbols, $\rho \equiv \rho^{(F)}$) obtained from Monte Carlo simulation for different interactions between polymer segments: $\varepsilon^{(PP)} = \varepsilon$ (circles), $\varepsilon^{(PP)} = 0.5\varepsilon$ (squares). Parameters: $\varepsilon^{(FF)} = \varepsilon^{(FP)} = \varepsilon$, $\rho_P\sigma^2 = 0.099\,872$ and $\mu_b^{(F)}/\varepsilon = -4.0$. (b) Density profiles of polymers (void symbols, $\rho \equiv \rho_s^{(P)}$) and fluid (solid symbols, $\rho \equiv \rho^{(F)}$) obtained from Monte Carlo simulation. Parameters: $\varepsilon^{(PP)} = \varepsilon^{(FF)} = \varepsilon$ and $\varepsilon^{(FP)} = 1.5\varepsilon$, $\rho_P\sigma^2 = 0.099\,872$ and $\mu_b^{(F)}/\varepsilon = -4.0$. Note that the Dirac delta function contribution to the density profiles $\rho_s^{(P)}(z)$ is omitted for the sake of a better visualization.

interactions are compared. The density profiles of polymers shown here are similar. However, reduction of attraction between segments causes a considerable increase in the fluid density inside the brush. This can be easily explained in a heuristic manner. When segment−segment interactions are weaker, a "sticking" of spherical molecules to the chains becomes more probable. In part b, the structure of the system with the higher "sticking" energy parameter ($\varepsilon^{(FP)} = 1.5\varepsilon$) is shown. In this case the fluid density in the surface region is higher than that in the bulk part of the system. Moreover, the fluid density achieves the bulk value at a distance z greater than the effective thickness of the brush.

To some extent the density profiles of spherical molecules repeat the pattern of the relevant density profile of polymers. In the case of high grafting densities, the fluid density profiles exhibit several sharp peaks. For small amount of grafted polymers, well-pronounced peaks are not observed. Moving further outward from the wall, one sees that the density of fluid gradually tends to the bulk value and achieves it at a distance z considerably greater than the effective brush height. In some cases, fluid molecules not only penetrate the bonded phase but also adsorb "on the brush" (see Figure 5b).

The proposed density functional approach well approximates simulation data for denser systems. The differences between theoretical predictions and simulation results appear for low densities of polymers and spherical molecules.

Now we use the density functional theory to analyze adsorptive properties of the surfaces with chemically bonded phases. As seen in Figure 6 the excess adsorption of fluid molecules depends on the length of the polymer chains and the grafting density. For low bulk densities of fluid, adsorption increases with an increase of chain length, but the opposite effect is observed for higher values of $\rho_b^{(F)}$. The change in the sequence of adsorption isotherms appears at lower fluid density for denser bonded-phase grafting density. Obviously, adsorption increases when the parameter $\varepsilon^{(FP)}$ increases (Figure 7). The relation between excess adsorption of Lennard-Jones fluid and grafting density is shown in Figure 8. With increasing grafting density the excess adsorption increases, attains its maximum value, and then smoothly decreases.

A Density Functional Approach to Retention in Chromatographic Systems. The considered approach can be used to modeling the retention process in chromatography with chemically bonded phases. One can divide the system into two

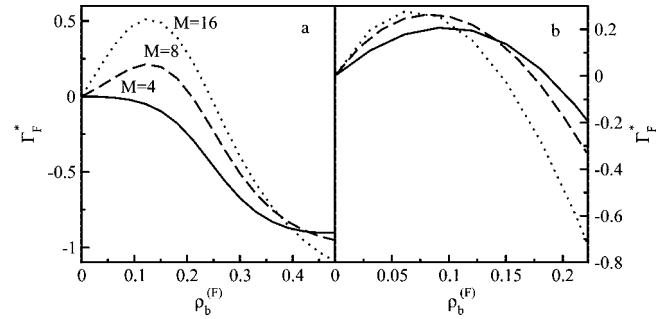

Figure 6. Theoretical excess adsorption ($\Gamma^* = \Gamma\sigma^2$) isotherms for different chain lengths: $M = 4$ (solid line), 8 (dashed line), and 16 (dotted line). Parameters: $\varepsilon^{(FF)} = \varepsilon^{(PP)} = \varepsilon^{(FP)} = \varepsilon$ and (a) $\rho_P\sigma^2 = 0.05$, (b) $\rho_P\sigma^2 = 0.3$. The numbers of segments are given in the part a.

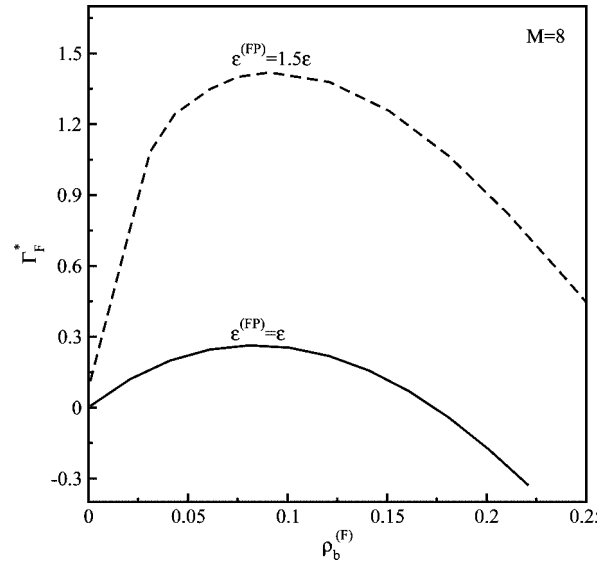

Figure 7. Theoretical excess adsorption ($\Gamma^* = \Gamma\sigma^2$) isotherms. Parameters: $M = 8$, $\rho_P = 0.3$, $\varepsilon^{(FF)} = \varepsilon^{(PP)} = \varepsilon$, $\varepsilon^{(FP)} = \varepsilon$ (solid line), and $\varepsilon^{(FP)} = 1.5\varepsilon$ (dashed line). The values of $\varepsilon^{(FP)}$ are given in the figure.

phases: the stationary phase (surface phase) and the mobile (bulk) phase. The location of the dividing surface is rather arbitrary and various methods for its estimation have been used in refs 48, 49, 59, 62, and 63. When both phases are well-defined, we can analyze the distribution of the fluid molecules between the stationary and mobile phases. The distribution coefficient, K_F, is defined by the ratio of fluid (solute) densities in the stationary and mobile phases

$$K_F = \rho_{stat}^{(F)}/\rho_b^{(F)} \tag{19}$$

where $\rho_{stat}^{(F)}$ is the average fluid density in the stationary phase

$$\rho_{stat} = (1/z_0)\int_0^{z_0} \rho^{(F)}(z)\,dz \tag{20}$$

and z_0 denotes a position of the dividing surface. We have estimated the value of z_0 inspecting density profiles of spherical molecules and have used the value, at which the local density, $\rho^{(F)}$, differs from its bulk value no more than by 1%. By multiplying the distribution coefficient by the ratio of volumes of the two phases one obtains the retention factor k'_F, which can be experimentally measured.[48]

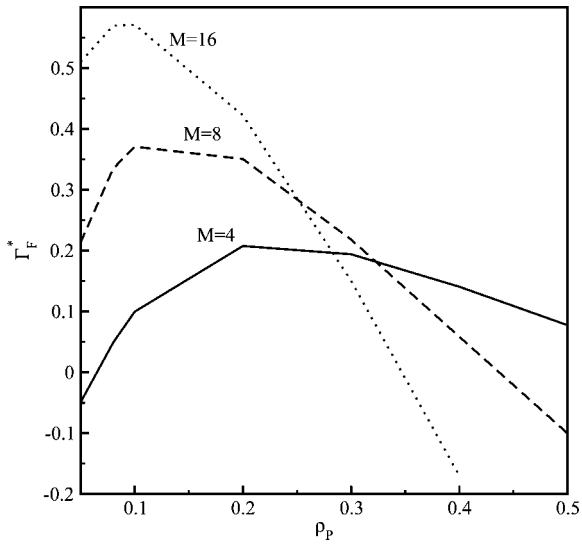

Figure 8. Theoretical excess adsorption ($\Gamma^* = \Gamma\sigma^2$) as function of the grafting density for different chain lengths: $M = 4$ (solid line), 8 (dashed line), and 16 (dotted line). Parameters: $\varepsilon^{(FF)} = \varepsilon^{(PP)} = \varepsilon^{(FP)} = \varepsilon$ and $\rho_b^{(F)}\sigma^3 = 0.121$. The numbers of segments are given in the figure.

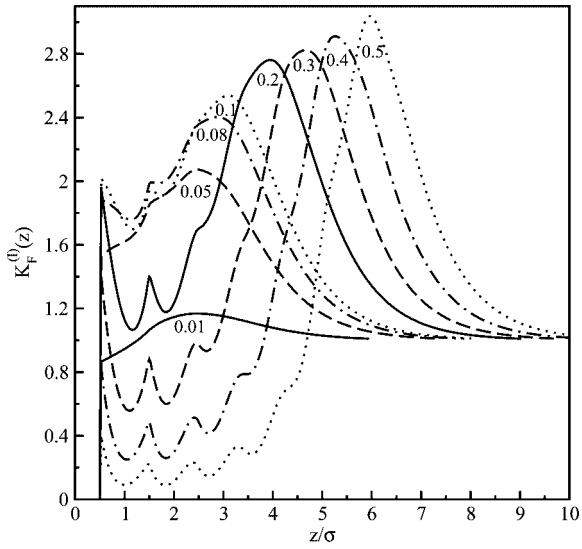

Figure 9. Theoretical distribution coefficient profiles for different grafting densities, given in the figure. Parameters: $M = 8$, $\varepsilon^{(FF)} = \varepsilon^{(PP)} = \varepsilon^{(FP)} = \varepsilon$, and $\rho_b^{(F)}\sigma^3 = 0.1$.

It is also convenient to define "the local distribution coefficient" as[62]

$$K_F^{(l)}(z) = \rho^{(F)}(z)/\rho_b^{(F)} \tag{21}$$

Examples of functions $K_F^{(l)}(z)$ are shown in Figure 9 for different grafting densities. For extremely low grafting densities the profile $K_F^{(l)}(z)$ exhibits one maximum in the middle region of the surface layer. When the bonded phase is denser, on the function $K_F^{(l)}(z)$ appear a maximum located near the surface, a deep minimum in the middle part of the brush and a high maximum in its outer region. Figure 10 presents the local distribution coefficients for different polymer−fluid interactions. As seen here, the attraction between polymer chains and spherical molecules strongly heightens the values of $K_F^{(l)}(z)$.

Figure 11 shows the dependence of the distribution coefficient K_F on the grafting density. At low grafting densities, the value

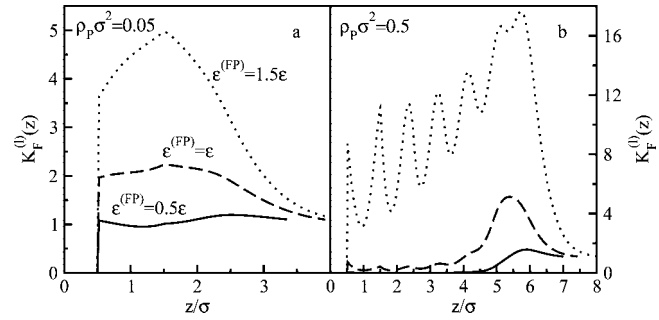

Figure 10. Theoretical distribution coefficient profiles for different energy parameters $\varepsilon^{(FP)} = 0.5\varepsilon$ (solid lines), ε (dashed lines), and 1.5ε (dotted lines). The values of $\varepsilon^{(FP)}$ are given in the figure. Parameters: $M = 8$, $\varepsilon^{(FF)} = \varepsilon^{(PP)} = \varepsilon$, $\rho_b^{(F)}\sigma^3 = 0.01$ and (a) $\rho_P\sigma^2 = 0.05$, and (b) $\rho_P\sigma^2 = 0.5$.

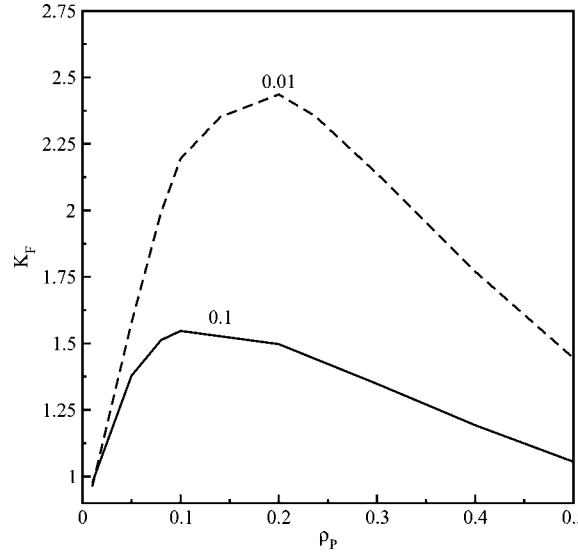

Figure 11. Theoretical dependencies of the distribution coefficient on the grafting density. Parameters: $M = 8$, $\varepsilon^{(FF)} = \varepsilon^{(PP)} = \varepsilon^{(FP)} = \varepsilon$, and $\rho_b^{(F)}\sigma^3 = 0.1$ (solid line) and 0.01 (dashed line). The values of $\rho_b^{(F)}\sigma^3$ are given in the figure.

of K_F increases with the surface coverage of the grafted chains. It reaches a maximum at the point where interactions between polymer chains become significant and hinder penetration of the brush. For higher grafting density, K_F decreases because of increasing entropic expulsion of fluid molecules by the grafted polymers. This type of dependence between the coefficient K_F and the grafting density is observed in experiments.[67−70] As one can see in Figure 11, the distribution coefficient strongly depends on the bulk density. In chromatographic applications, extremely low solute concentrations are used.

One of the important factors used to optimize chromatographic separation is the selectivity, defined as the ratio of the distribution coefficients of two solutes, $\alpha = K_1/K_2$. The effect of grafting density on the selectivity is shown in Figure 12. The considered solutes have different affinities to the stationary phase (different energy of solute−polymer interactions, $\varepsilon^{(FP)}$). The selectivity achieves the maximum value at a mediate grafting density, and slightly decreases with further increase of the number of grafted chains on the surface. Additionally, the distribution coefficient for the solute that is less attracted by the chains reaches its maximum at lower grafting density than the other one (see the inset in Figure 12). These findings agree with experimental data[68−70] and the results of computer simulations.[62,63]

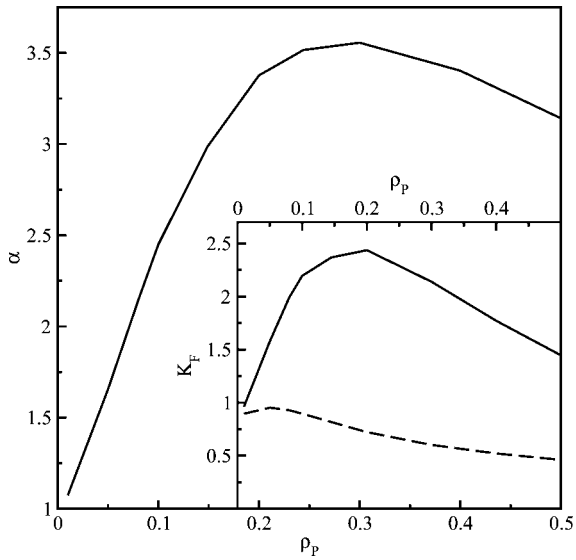

Figure 12. Theoretical dependence of the selectivity $\alpha = K_1/K_2$ on the grafting density. For the solute 1, $\varepsilon^{(FP)} = \varepsilon$, whereas for the solute 2, $\varepsilon^{(FP)} = 0.5\varepsilon$. Parameters: $M = 8$, $\varepsilon^{(FF)} = \varepsilon^{(PP)} = \varepsilon$, and $\rho_b^{(F)}\sigma^3 = 0.01$.

The theory presented above can be used for gas and liquid chromatography with chemically bonded phases. The eluant (gas or liquid mixture) can be incorporated to the model in the framework of "continuum-solvent" approximation.[22−27]

Effects of such a "virtual" solvent are modeled by assuming the suitable energy parameters $\varepsilon^{(FF)}$, $\varepsilon^{(PP)}$, and $\varepsilon^{(FP)}$. When effective interactions between segments are strongly attractive, the collapse of chains is observed. This situation corresponds to a "poor solvent" regime. However, for weak interactions between segments, solvent−segment contact can be more favorable. In such a "good solvent" the chains are stretched in a direction perpendicular to the wall (see Figures 1 and 2). In reversed phase chromatography mixtures of organic solvents with water are usually used as the mobile phase. Their eluotropic strength depends on the mixture composition. However, with a crude approximation we can characterize a given mixed-solvent using parameter $\varepsilon^{(PP)}$. The density functional theory presented here captures fundamental properties of solute distribution between the stationary and mobile (bulk) phases.

VI. Summary

We have applied the functional density theory to study adsorption of Lennard-Jones fluid on chemically modified surfaces. We have shown how various parameters affect the structure of bonded phase, the density profiles of spherical molecules, and the excess adsorption isotherms of the fluid in the considered systems. We have found that depending on the grafting density and interaction parameters, the small molecules adsorb in the outer part of the polymer film or penetrate the brush. Moreover, we have shown that with increasing grafting density the excess adsorption increases to the maximum value and then smoothly decreases. We have also calculated adsorption isotherms for surfaces modified with chains of different lengths. Adsorption of a dilute fluid is higher on the surfaces covered by longer chains; however, for the dense fluid adsorption decreases with increasing the chain length. It has been demonstrated that our theoretical approach leads to a quite good agreement with Monte Carlo simulation data.

We have also proposed an extension of this approach to describe the distribution of spherical molecules between the surface and bulk phase. We have involved the solvent-free model of the system. However, our studies clearly demonstrate that even such a simple model, solved in the framework of the density functional theory, can describe the most salient features of the retention process.

In this study, we have restricted our attention to simple situation in which a bare surface is "inert" with respect to polymers and spherical molecules. The hard wall affects chain segments only entropically via purely geometrical restrictions. Obviously, attractive interactions of segments and spherical molecules with the surface would change the structure of the brush and, as a consequence, affect adsorption of the fluid. Our theoretical treatment can be also used to study such systems. The limitations of the model and theory have been already discussed in ref 33. However, in our opinion the proposed density functional approach is a good tool to get insight into behavior of various interfacial systems.

References and Notes

(1) Netz, R. R.; Andelman, D. *Phys. Rep.* **2003**, *380*, 1.
(2) Liakos, I. L.; Newman, R. C.; McAlpine, E.; Alexander, M. R. *Surf. Interface Anal.* **2004**, *34*, 347.
(3) Weaver, J. F.; Carlsson, A. F.; Madix, R. J. *Surf. Sci. Rep.* **2003**, *50*, 107.
(4) Carlsson, A. F.; Madix, R. J. *J. Phys. Chem. B* **2001**, *105*, 8155.
(5) Alexander, S. *J. Phys. (Fr.)* **1977**, *38*, 983.
(6) de Gennes, P. G. *Macromolecules* **1980**, *13*, 1069.
(7) Milner, S. T.; Witten, T. A.; Cates, M. E. *Europhys. Lett.* **1988**, *5*, 413.
(8) Milner, S. T.; Witten, T. A.; Cates, M. E. *Macromolecules* **1988**, *21*, 2610.
(9) Milner, S. T. *Science* **1991**, *251*, 905.
(10) Zhalina, E. B.; Borisov, O. V.; Pryamitsyn, V. A.; Birshtein, T. M. *Macromolecules* **1991**, *24*, 140.
(11) Shim, D. F. K.; Cates, M. E. *J. Phys. (Fr.)* **1989**, *50*, 3535.
(12) Whitmore, M. D.; Noolandi, J. *Macromolecules* **1990**, *23*, 3321.
(13) Patra, C. N.; Yethiray, A.; Curro, J. G. *J. Chem. Phys.* **1999**, *111*, 1608.
(14) Leermakers, F. A. M.; Philipsen, H. J. A.; Klumperman, B. *J. Chromatogr. A* **2002**, *959*, 37.
(15) Stoyanov, S. D.; Paunov, V. N.; Rehage, H.; Kuhn, H. *Phys. Chem. Chem. Phys.* **2004**, *6*, 596.
(16) Manciu, M.; Ruckenstein, E. *Langmuir* **2004**, *20*, 6490.
(17) Pang, P.; Koska, J.; Coad, B. R.; Brooks, D. E.; Haynes, C. A. *Biotechnol. Bioeng.* **2005**, *90*, 1.
(18) Carignano, M. A.; Szleifer, I. *J. Chem. Phys.* **1994**, *100*, 3210.
(19) Carignano, M. A.; Szleifer, I. *Macromolecules* **1995**, *28*, 3197.
(20) Carignano, M. A.; Szleifer, I. *J. Chem. Phys.* **1995**, *102*, 8662.
(21) Szleifer, I.; Carignano, M. A. *Adv. Chem. Phys.* **1996**, *XCIV*, 165.
(22) McCoy, J. D.; Ye, Y.; Curro, J. G. *J. Chem. Phys.* **2002**, *117*, 2975.
(23) Ye, Y.; McCoy, J. D.; Curro, J. G. *J. Chem. Phys.* **2003**, *119*, 555.
(24) Hooper, J. B.; McCoy, J. D.; Curro, J. G.; van Swol, F. *J. Chem. Phys.* **2000**, *113*, 2021.
(25) McCoy, J. D.; Teixeira, M. A.; Curro, J. G. *J. Chem. Phys.* **2001**, *113*, 4289.
(26) Cao, D. P.; Wu, J. *Langmuir* **2006**, *22*, 2712.
(27) Jiang, T.; Li, Z.; Wu, J. Z. *Macromolecules* **2007**, *40*, 334.
(28) Yu, Y. X.; Wu, J. *J. Chem. Phys.* **2002**, *117*, 2368.
(29) Yu, Y. X.; Wu, J. *J. Chem. Phys.* **2002**, *117*, 10165.
(30) Yu, Y. X.; Wu, J. *J. Chem. Phys.* **2003**, *118*, 3835.
(31) Borǒwko, M.; Rzysko, W.; Sokołowski, S.; Staszewski, T. *J. Chem. Phys.* **2007**, *126*, 214703.
(32) Matusewicz, A.; Patrykiejew, A.; Sokołowski, S.; Pizio, O. *J. Chem. Phys.* **2007**, *127*, 174707.
(33) Patrykiejew, A.; Sokołowski, S.; Tscheliessnig, R.; Fischer, J.; Pizio, O. *J. Phys. Chem. B* **2008**, *112*, 4552.
(34) Grest, G. S.; Murat, M. *Macromolecules* **1993**, *26*, 3108.
(35) Lai, P. Y.; Binder, K. *J. Chem. Phys.* **1991**, *95*, 9288.
(36) Lai, P. Y.; Binder, K. *J. Chem. Phys.* **1992**, *97*, 586.
(37) Lai, P. Y. *J. Chem. Phys.* **1993**, *98*, 669.
(38) Weinhold, J. D.; Kumar, S. K. *J. Chem. Phys.* **1994**, *101*, 4312.
(39) Grest, G. S. *J. Chem. Phys.* **1996**, *105*, 5532.
(40) Pastorino, C.; Binder, K.; Keer, T.; Mueller, M. *J. Chem. Phys.* **2006**, *124*, 064902.
(41) Ohno, K.; Sakamoto, T.; Minagawa, T.; Okabe, Y. *Macromolecules* **2007**, *40*, 723.

(42) Descas, R.; Sommer, J. U.; Blumen, A. *J. Chem. Phys.* **2006**, *125*, 214702.
(43) Wongkoblap, A.; Do, D. D. *J. Colloid Interface Sci.* **2006**, *297*, 1.
(44) Patra, M.; Linse, P. *Nano Lett.* **2006**, *6*, 133.
(45) Mueller, M.; MacDowell, L. G. *J. Phys.: Condens. Matter* **2003**, *15*, R609.
(46) MacDowell, L. G.; Mueller, M. *J. Chem. Phys.* **2006**, *124*, 084907.
(47) Neue, U. D. *HPLC Columns: Theory, Technology and Practice*; Wiley-Interscience: New York, 1997.
(48) Dorsey, J. H.; Dill, K. A. *Chem. Rev.* **1989**, *89*, 331.
(49) Martire, M. E.; Boehm, R. E. *J. Phys. Chem.* **1983**, *87*, 1045.
(50) Bohmer, M. R.; Koopal, L. K.; Tijssen, R. *J. Phys. Chem.* **1991**, *92*, 6285.
(51) Tijssen, R.; Schoenmakers, P. J.; Bohmer, M. R.; Koopal, L. K.; Boliet, H. A. H. *J. Chromatogr. A* **1993**, *656*, 135–5546.
(52) Klatte, S. J.; Beck, T. L. *J. Chem. Phys.* **1993**, *97*, 5727.
(53) Klatte, S. J.; Beck, T. L. *J. Chem. Phys.* **1995**, *99*, 16024.
(54) Yarovsky, I.; Aguilar, M. I.; Hearn, M. T. W. *Anal. Chem.* **1996**, *68*, 1974.
(55) Lippa, K. A.; Sander, L. C.; Mountain, R. D. *Anal. Chem.* **2005**, *77*, 7862.
(56) Klatte, S. J.; Beck, T. L. *J. Chem. Phys.* **1996**, *100*, 5931.
(57) Sluster, J. T.; Mountain, R. D. *J. Phys. Chem. B* **1999**, *103*, 1354.
(58) Ban, K.; Saito, Y.; Jinno, K. *Anal. Sci.* **2005**, *21*, 397.
(59) Zhang, L.; Rafferty, J. L.; Siepmann, J. I.; Chen, B.; Schure, M. R. *J. Chromatogr. A* **2006**, *1126*, 219.
(60) Rafferty, J. L.; Zhang, L.; Siepmann, J. I.; Schure, M. *R Anal. Chem.* **2007**, *79*, 6551.
(61) Rafferty, J. L.; Siepmann, J. I.; Schure, M. R. *J. Chromatogr. A* **2008**, *1204*, 11.
(62) Rafferty, J. L.; Siepmann, J. I.; Schure, M. R. *J. Chromatogr. A* **2008**, *1204*, 20.
(63) Rafferty, J. L.; Siepmann, J. I.; Schure, M. R. *Anal. Chem.* **2008**, *80*, 6214.
(64) Weeks, J. D.; Chandler, D.; Andersen, H. C. *J. Chem. Phys.* **1971**, *54*, 5237.
(65) Frenkel, D.; Smit, B. *Understanding Molecular Simulation form Algorithms to Applications*; Academic Press: San Diego, CA, 1996.
(66) Rosenbluth, M. N.; Rosenbluth, A. W. *J. Chem. Phys.* **1955**, *23*, 356.
(67) Hennion, M. C.; Picard, C.; Caude, M. *J. Chromatogr.* **1978**, *166*, 21.
(68) Sentell, K. B.; Dorsey, J. G. *Anal. Chem.* **1989**, *61*, 930.
(69) Miyabe, K.; Guiochon, G. *J. Chromatogr. A* **2000**, *903*, 1.
(70) Gritt, F.; Guiochon, G. *J. Chromatogr. A* **2006**, *1115*, 142.

JP811143N